Incorporation of CdS nanoparticles on mesoporous silicon substrate as application for detection systems.

Fatima Saker
Laboratoire des Matériaux et Structure des Systèmes Electromécaniques et leur Fiabilité LMSSEF
Larbi Ben M'hidi Univercity
Oum El Bouaghi, Algeria
sfphysique@hotmail.fr

Louardi Remache
Laboratoire des Matériaux et Structure des Systèmes Electromécaniques et leur Fiabilité LMSSEF
Larbi Ben M'hidi Univercity
Oum El Bouaghi, Algeria
rlouardi@yahoo.fr

Abdellah Rahmani
Laboratoire des Matériaux et Structure des Systèmes Electromécaniques et leur Fiabilité LMSSEF
Larbi Ben M'hidi Univercity
Oum El Bouaghi, Algeria
https://orcid.org/0000-0001-7883-4759

Hassiba Moualkia
Laboratoire des Matériaux et Structure des Systèmes Electromécaniques et leur Fiabilité LMSSEF
Larbi Ben M'hidi Univercity
Oum El Bouaghi, Algeria
moualkia@yahoo.fr

Abstract—**in this study CdS nanoparticles were successfully deposited by chemical bath deposition (CBD) on the porous silicon (Psi) and glass substrates. In order to prepare porous silicon, an electrochemical etching method was carried out using p-type Si (100) at various current densities with fixed time (5 min). Crystallographic structure of prepared samples was analyzed with X-ray diffraction (XRD), The surface morphology of films was obtained by scanning electron microscopy (SEM). Results demonstrated that the morphology of the deposited materials was influenced by the porosityof the PSi substrate. The crystallite size determined by the Debye-Scherrer equation and the smallest value was 13.96 nm from CdS/PSi anodized using the current density of 60 mA/cm^2.SEM results confirms the shows the porous CdS thin films morphology. The optical properties of nanostructure CdS thin films were obtained by using UV-visible. TheCdS shows a band gap(E_g=2.3 eV)valueobtained by transmittancespectrum. The high surface area of CdS/PSi structures could be helpful for making highly sensitive photodetectors.**

Keywords—Porous silicon(PSi),CdS,nanoparticles, photodetector.

I.INTRODUCTION

Cadmium sulfide CdS has a direct band gap semiconductor of 2.42 eV at room temperature. And is one of the most important II-VI semiconductors used in the electronic and optoelectronic field [1].

CdSthin films can be deposited by different deposition techniques such as spray pyrolysis, thermal evaporation, chemical bath deposition, pulsed laser deposition, dip coating etc[1-5].Among these methods, the chemical bath deposition (CBD) is very simple and inexpensive method, it can be used to produce large area homogeneous films.

On the other hand, porous silicon has become a promising material for detection applications because of many reasons: its morphology, large specific surface area, low energy consumption, and its compatibility with silicon-based technologies[6-7]. In addition, the various morphological and structural properties of this material can be produced in a localized manner by a low-cost electrochemical process which can be integrated with microtechnological processes on silicon[6]. The sensitivity of PSi depends on the morphological characteristics of pores, including pore diameter,uniformity, surface smoothness and layer thickness [8]. Furthermore, its large specific surface area makes it more reactive than bulk silicon, which allows it to adapt to a large number of environmental and biochemical detection systems[9-10]. Many studies have been reported on improving the performance of porous silicon-based detectors[6-11]. specially to manufacture high-performance photo-detectors[6].Another more attractive way, that which consists in introducing nanoparticles of materials in the PSi matrix, this process makes it possible to improve the electrical properties of the elaborated layers and to manufacture sensors having higher and faster response[12].In this context, several materials can be incorporated into the PSi matrix like: ZnO, ZnS, TiO_2 ...and others more[13-14].

Several studies have been reported on the incorporation of nanoparticles into the matrix of PSi, and among the materials that can be integrated into the matrix of porous silicon, CdSe, CdS, ZnS, ZnO etc. S.A.Hasoon&al also made studies on fabrication of nanostructure CdS thin films deposited by vacuum thermal evaporation technique on PSi matrix[5]. Sara.T &al are fabricated CuS /PSi heterojunction photodetector using chemical spray pyrolysis route[4]. Khashan described the improvement of PSi photo-detectors when they are incorporated with ZnO nanoparticles prepared by a chemical method[15].N.F.Habubi described the response improvement of PSi photo-detectors when they are incorporated with CdSe nanoparticles prepared by laser ablation[16].

Yong Li & al [1]have studies the electronic properties of CdS/Si nano-heterostructure prepared by CBD on the silicon nanoporous pillar array.

This work aims to study the incorporation of CdSnanoparticles on the PSi matrix by using the chemical bath deposition (CBD)method. The effect of the PSi

substrate on the structural, morphological and optical properties of the CdS layers was investigated by comparing to the CdS/Glass structure.

II. EXPERIMENTAL METHOD

Preparation of PS matrix

The PSi layers were prepared by anodizing of p-type Boron doped(100) oriented monocrystalline silicon(C.Si) wafer , with resistivity0.015-0018 Ωcm and thickness of 250-300µm in hydrofluoric acid and ethanol with platinum electrode as cathode. The electrolyte was prepared by mixing HF with concentration (40%) and ethanol (C_2H_5OH99.98%) with the ratio of 1:1 by volume using a single-cell connected with keithley model 4200. The porous layers were prepared at various current densities of (30 and 60) mA/cm^{2}during5 min at room temperature where the porosity of PSi was 35% and 55% respectively
Finally, the samples were taken out and washed with ethanol and dried by hair dryer. The silicon wafers were cleaned in HF 2 % before the anodization process.

Incorporation of CdS nanoparticles

CdS thin films were deposited on the PSi and on glass using a CBD method. The used solution was a mixture of cadmium sulfate ($CdSO_4$), Ammonia (NH_4OH),Thiourea **(**$CS(NH_2)_2$and Deionized water (DI H_2O), where it was placed into the bath fixed at 50°C, next NH_4OH, $CdSO_4$ and**(**$CS(NH_2)_2$ were added to the (DI H_2O) for 60 min with a magnetic agitation to homogenize the mixture. The samples were taken out and washed thoroughly with de-ionization water and dried by hair dryer. As-grown CdS thin films were homogeneous, yellowish, and with good adherence to glass and PSi.

In this study, we have three samples: CdS nanoparticules deposited on glass (CdS/glass) and on porous silicon fabricated at 30mA/cm^2 (CdS30) and 60 mA/cm^2 (CdS60)during 5 min. The crystallographic structure of the prepared samples was analyzed with X-ray diffraction (XRD) using ARL-EQUINOX 100 X-ray diffractometer (CuKα1 radiation, 40 mA, 40KV) in the range of (10-90 deg).Optical transmittance and surface morphology of the CdS nanoparticles were investigated by means of a UV–visible spectrophotometer Jacso V-30 and (TESCAN VEGA3) scanning electron microscopy (SEM) .

III. RESULT AND DISCUSSION

III.1 Structural characterizations:

Fig.1 illustrates the XRD patterns of CdS nanoparticles deposited on glass and porous silicon substrates.
The X-ray diffraction (XRD) analysis indicates that CdS/glass and CdS/PSi thin films showed the cubic crystalline phase.
CdS/glass have showed peak at 26.6°corresponding to the (111) and small peaks at 29.9°, 44.2° and 52.4°corresponding to the (200), (220) and (311) orientations of CdS according to (COD ID:900108).
The patterns of CdS/SiP contain several diffraction peaks at 26.6°,29.9°,44.1°,51.7°corresponding to (111), (200), (220),(311), plane, respectively, belonging to the CdS cubic phase. When the peaks at 32.2° and 55.1 ° are corresponding to (111), (202) of CdO cubic phase according to (COD ID: 1011051).
The appearance of CdO can be explained by the oxidation of the CdS films at the levels of the silicon pores.
the layers deposited on PSi are more intense (almost x 4) compared to that deposited on glass, which shows the improvement of the CdS layers crystallization using porous silicon substrates. This amelioration is due to the good crystallization of the PSi substrates, on the other hand, the glass substrate is amorphous, which allows us to confirm the effect of the substrate type on the deposited layer of CdS. The structure obtained for samples CdS30 and CdS60 is similar to the results of other studies[17-18], which is maybe the structure of mixed phase that starts from the cubic and tends towards the hexagonal phase via annealing. This structure maybe becomes a hexagonal phase after annealing.

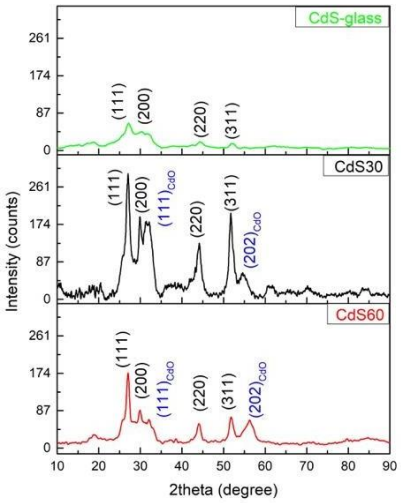

Fig. 1. XRD spectra of CdS nanoparticles deposited on glass and on porous silicon.

The grain size D is calculated using Debye Scherer's formula[19]:

$$D = \frac{K.\lambda}{\beta.\cos\theta} (1)$$

Where:
D: the grain size.
β : the full width at half maximum (FWHM in radians) of thepeak corrected for instrumental broadening
θ: the position of the diffraction peak considered.
K: Scherer constant, this value is taken as 0.9 for the calculations
λ: the wavelength of the X-ray.
The distances are expressed in [Å] and the angles in radians. the strain values ε can be calculated using the following formula [5]:

$$\varepsilon = \frac{\beta\cos\theta}{4} (2)$$

The dislocation density δ is deduced using the relation of Williamson and Smallman's [20]:

$$\delta = \frac{1}{D^2} (3)$$

In the table 1 we listed the XRD data and results for CdS/glass and CdS/Psi.

The calculated particle size showed that it was related to the nature of the substrate, as it took a lower value when replacing the glass substrate with the porous silicon substrate. It was also affected by the porosity ofthe porous silicon substrate, where we noticed that the crystallite size decreases when the porosity increases.

TABLE I. structural parameters of CdS nanoparticles deposited on glass and porous silicon substrates

templates	CdS/glass			CdS/PSi					
				CdS30			*CdS60*		
hkl	111			111	202	311	111	202	311
2 θ(°)	26.635			26.679	44.171	51.734	27.095	44.055	5.838
2 θ(°)REF	26.445			26.445	43.866	51.951	26.445	43.866	51.951
Δθ(°)	0.190			0.234	0.305	0.217	0.650	0.189	0.113
FWHM(°)	0.177			0.295	0.413	0.295	0.472	0.708	0.708
Crystallite size D (nm)	46.113			27.671	20.753	29.921	17.309	12.101	12.472
D_{midum} (nm)	46.116			26.115			13.960		
$d_{spacing}$(nm)	0.335	0.204	0.174	0.335	0.204	0.176	0.332	0.206	0.176
d(nm)REF	0.337	0.206	0.176	0.337	0.176	0.176	0.337	0.176	0.176
(δ)x10^{-3}(nm^{-2})	1.518			1.466			5.131		
(ε)x10^{-3}	0.751	2.860	1.847	1.252	1.669	1.158	2.001	2.863	2.778

III.2 Morphological study:

Figure 2 shows the SEM images of CdS thin films deposited on the PSi substrates from two different porosities (35% and 55%)

It can be seen that the structure consists of nanosheets with a vertical orientation, overlapped between them creating a porous morphology. The pores created have a polygonal shape, they are randomly distributed on the surface. The CdS60 has higher pore numbers than the other substrate; this result may be due to the porosity of CdS60, which is higher thanCdS30. We can distinguish clusters of round particles with a diameter from 300 nm to 400 nm on the walls of the pores.

This porous morphology makes the CdS / PSi structure a good candidate for detection systems (Photo-detection and gas sensors), because of the large specific surface area.

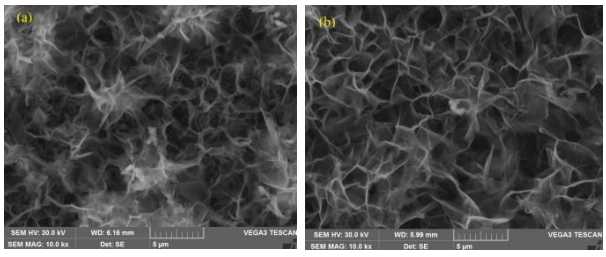

Fig.2. SEM image of CdS thin films deposited on the porous silicon: (a) CdS30, (b) CdS60.

III.3 Optical study:

Figure 3 shows the transmittance as a function of the wavelength for the CdS thin film deposited on glass.

In the wavelength range between 500 and 1000 nm, the transmittance varies between 25 and 55%.Theweak transmittance of the deposited film may be due tothe roughness surface because of the cluster's morphology of the CdS thin films.

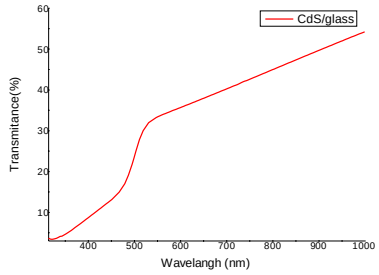

Fig.2. optical transmittance spectrum of CdS nanoparticles

The relation between the energy of the photon andtheoptical absorption coefficient (α) For direct transitions is expressed by the following relation [21], [22]:

$$A(h\nu)= A(h\nu- E_g)^{1/2} \quad (4)$$

Where:

A: constant

Eg: the optical gap [eV]

hν : the energy of a photon.

By scanning the entire energy domain, we have plotted $(\alpha h\nu)^2$ as a function of the energy of the photon E = hν (knowing that: $h\nu\ (eV) = \frac{hc}{\lambda} = \frac{12400}{\lambda(A°)}$ and extend the linear part of $(\alpha h\nu)^2$ up to the x-axis, we obtain the value of Eg (fig.4.)

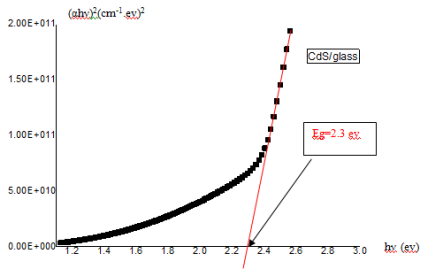

Fig. 4. Determination of the energy gap by extrapolation from the variation of $(\alpha h\nu)^2$ as a function of hν for a thin film of CdS

Fig.4 shows the optical band gap (E_g) of the CdS nanoparticles value for the simple CdS/glass
The value obtained of the energy band gap for the thin film of CdS deposited on glass is 2.3 eV.This value corresponds to what has been found by others[1].

CONCLUSION

Porous silicon layers were fabricated by the electrochemical etching method. CdS nanoparticles were deposited by chemical bath deposition. The XRD spectrum indicated that the CdS thin films have a cubic crystalline phase. The influence of porosity on the CdS nanoparticles properties, including structural and morphological properties, was investigated. CdS60 had the smallest value of particle size,it was around 13.9 nm. The value of the energy band gap of CdS was 2.3 eV.

REFERENCES

[1] Y. Li *et al.*, "Characterization of electronic structures from CdS/Si nanoheterostructure array based on silicon nanoporous pillar array,"*Materials Research Bulletin*, vol. 74, pp. 507–510, Feb. 2016, doi: 10.1016/j.materresbull.2015.11.023.

[2] N. P. Huse, A. S. Dive, K. P. Gattu, and R. Sharma, "An experimental and theoretical study on soft chemically grown CuS thin film for photosensor application,"*Materials Science in Semiconductor Processing*, vol. 67, pp. 62–68, Aug. 2017, doi: 10.1016/j.mssp.2017.05.010.

[3] S. Yadav and P. K. Bajpai, "Effect of Substrate on CuS/PVA Nanocomposite Thin Films Deposited on Glass and Silicon Substrate,"*SNL*, vol. 08, no. 02, pp. 9–19, 2018, doi: 10.4236/snl.2018.82002.

[4] S. T. Kassim, H. A. Hadi, and R. A. Ismail, "Fabrication and characterization of high photosensitivity CuS/porous silicon heterojunction photodetector,"*Optik*, vol. 221, p. 165339, Nov. 2020, doi: 10.1016/j.ijleo.2020.165339.

[5] S. A. Hasoon, I. M. Ibrahim, R. M. Al-Haddad, and S. S. Mahmood, "Fabrication of nanostructure CdS thin film on nanocrystalline porous silicon,"*International Journal of Current Engineering and Technology*, vol. 4, no. 2, pp. 594–601, 2014.

[6] N. Naderi and M. R. Hashim, "Effect of Surface Morphology on Electrical Properties of Electrochemically-Etched Porous Silicon Photodetectors,"*Int. J. Electrochem. Sci.*, vol. 7, p. 7, 2012.

[7] N. Ghellai, A. Chiali, N. E. Chabane-Sari, and N. Gabouze, "Etude et réalisation de capteurs de gaz à base de silicium poreux,"*Synthèse: Revue des Sciences et de la Technologie*, vol. 23, pp. 40–47, 2011.

[8] T. Jalkanen*et al.*, "Fabrication of porous silicon based humidity sensing elements on paper,"*Journal of Sensors*, vol. 2015, 2015.

[9] J. M. Buriak, "Organometallic Chemistry on Silicon and Germanium Surfaces,"*Chem. Rev.*, vol. 102, no. 5, pp. 1271–1308, May 2002, doi: 10.1021/cr000064s.

[10] A. Jane, R. Dronov, A. Hodges, and N. H. Voelcker, "Porous silicon biosensors on the advance,"*Trends in Biotechnology*, vol. 27, no. 4, pp. 230–239, Apr. 2009, doi: 10.1016/j.tibtech.2008.12.004.

[11] T. Jalkanen*et al.*, "Fabrication of Porous Silicon Based Humidity Sensing Elements on Paper,"*Journal of Sensors*, vol. 2015, pp. 1–10, 2015, doi: 10.1155/2015/927396.

[12] A. Rahmani, L. Remache, M. Guendouz, M. s. Aida, and Z. Hebboul, "Impact of the meso-PSi substrate on ZnO thin films deposited by spray pyrolysis technique for UV photodetectors,"*Appl. Phys. A*, vol. 127, no. 5, p. 396, May 2021, doi: 10.1007/s00339-021-04548-z.

[13] C.-M. Chou, H.-T. Cho, V. K. S. Hsiao, K.-T. Yong, and W.-C. Law, "Quantum dot-doped porous silicon metal–semiconductor metal photodetector,"*Nanoscale Res Lett*, vol. 7, no. 1, p. 291, Jun. 2012, doi: 10.1186/1556-276X-7-291.

[14] B. Meier, L. Egermann, S. Voigt, M. Stanel, H. Kempa, and A. C. Huebler, "Drift in the resistance of poly(3,4-ethylenedioxythiophene):poly(styrenesulfonate) printed films during thermal cycling,"*Thin Solid Films*, vol. 519, no. 19, pp. 6610–6612, Jul. 2011, doi: 10.1016/j.tsf.2011.04.225.

[15] K. S. Khashan, "OPTOELECTRONIC PROPERTIES OF ZnO NANOPARTICLES DEPOSITION ON POROUS SILICON,"*Int. J. Mod. Phys. B*, vol. 25, no. 02, pp. 277–282, Jan. 2011, doi: 10.1142/S0217979211054744.

[16] N. F. Habubi, R. A. Ismail, A. N. Abd, and W. K. Hamoudi, "Improved photoresponse of porous silicon photodetectors by embedding CdSe nanoparticles,"*IJPAP*, pp. 562–569, 2003.

[17] S. E. Haque, B. Ramdas, N. Padmavathy, and A. Sheela, "Facile one-pot low-temperature solid-state approach towards phase transformation of nanoCdS,"*Micro & Nano Letters*, vol. 9, no. 10, pp. 731–735, Oct. 2014, doi: 10.1049/mnl.2014.0167.

[18] J. Zhu *et al.*, "Highly efficient wurtzite/zinc blende CdS visible light photocatalyst with high charge separation efficiency and stability,"*J. Chem. Phys.*, vol. 152, no. 24, p. 244703, Jun. 2020, doi: 10.1063/5.0011132.

[19] V. G. Nair, R. Jayakrishnan, J. John, J. A. Salam, A. M. Anand, and A. Raj, "Anomalous photoconductivity in chemical spray pyrolysis deposited nano-crystalline ZnO thin films,"*Materials Chemistry and Physics*, vol. 247, p. 122849, Jun. 2020, doi: 10.1016/j.matchemphys.2020.122849.

[20] D. Komaraiah, E. Radha, Y. Vijayakumar, J. Sivakumar, M. V. R. Reddy, and R. Sayanna, "Optical, Structural and Morphological Properties of Photocatalytic ZnO Thin Films Deposited by Pray Pyrolysis Technique,"*Modern Research in Catalysis*, vol. 5, no. 4, Art. no. 4, Sep. 2016, doi: 10.4236/mrc.2016.54011.

[21] T. Güngör and H. Tolunay, "Drift mobility measurements in a-SiNx:H,"*Journal of Non-Crystalline Solids*, vol. 282, no. 2–3, pp. 197–202, Apr. 2001, doi: 10.1016/S0022-3093(01)00340-4.

[22] T. Gungor, "Ph. D. Thesis,"Hacettepe University, Department of Physics Engeneering, 2001.

Optical filters based on one dimensional dielectric photonic crystal defected by Magnetized cold plasma

Chouaib Chettah
Department of Petrochemical, University 20 August 1955-Skikda.
Hyperfrequency and Semiconductor Laboratory, University Frères Mentouri-Constantine1.
Constantine, Algeria.
chettah_chouaib@yahoo.fr &
c.chettah@univ-skikda.dz

Khaled Chettah
Department of Physics, University Frères Mentouri Constantine 1.
Research center in industrial technologies CRTI, Cheraga, Algiers.
Constantine, Algeria.
khaledphys25@gmail.com

Ouarda Barkat
Department of Electronics, University Frères Mentouri Constantine 1.
Electromagnetism and Telecommunications Laboratory, University Frères Mentouri Constantine 1.
Constantine, Algeria.
barkatwarda@yahoo.fr

***Abstract*— In this paper, a new analysis of optical selective filters containing one dimensional photonic crystal (1D-PC), magnetized cold plasma and dielectric materials are investigated using transfer matrix method. The effects of defective layers on transmission spectrum, the peak position and PBG are investigated as the function of the magnetic field and incidence angle.. It is found that the peak frequencies and the PBG are affected significantly by the magnetic field applied and number of defectives layers. Also, it is demonstrated that the plasma electron density of magnetized cold plasma layer has a significant effect on the transmission spectrum. Results obtained confirmed that it is possible to make a model of a highly selective tunable filter using photonic one dimensional plasma dielectric photonic crystal.**

Keywords— Transmission, Photonic Crystals, Magnetized cold plasma, Photonic Band Gap, Defectives layers

I. INTRODUCTION

Advances in plasma photonic crystal technology were encouraging in the realization of the optical filter [1-5]. It is an artificially periodic lattice composed of an alternation of thin non-magnetized or magnetized plasmas and dielectric materials. It is well known that non-magnetized plasma can be characterized by a complex frequency dependent permittivity medium. If an external magnetic field is introduced into plasma and low temperature photonic crystals, a new type of plasma photonic crystals called magnetized cold plasma photonic crystals (MCP-PCs) can be obtained [6-10].

MCP-PCs have attracted a lot of attention due to : their unique electromagnetic properties such as the ease of use of the external magnetic field, their magneto-optical effects based on the properties of PBGs and the ability to control the electron density of the plasma. Several studies suggest that MCP-PCs are emerging as new hot spots in photon engineering due to better control of the external magnetic field on PBGs. In this work, we study and analyze the transmittance as a function of the frequency of the one-dimensional periodic structure of the layers of indium arsenide (InAs) and silicon dioxide (SiO_2) [11,12] with a defective layer of Cold magnetized plasma (MCP) using the transfer matrix method (TMM) Fig.1. The optical constant of the MCP material is adjusted with varying parameters of the plasma. Therefore, we calculate the change in the transmittance of the structure with a defective MCP layer as a function of the angle of incidence, the electron density magnetic field and the thicknesses of the InAs and SiO_2 materials.

In addition, we calculate and compare the transmittance of the structures considered with one and two defective MCP layers. The frequency-dependent transmittance of the considered periodic multilayer structures is analyzed by inserting an MCP plasma layer in the symmetrical structure, for potential application in a tunable multichannel filter in the microwave region.

II. PROBLEM AND THEORY

Consider a one-dimensional photonic crystal structure (1D-PC), which is a periodic structure composed of a multilayer stack. This structure is symmetric in the form $(D_1D_2)^{N/2}$ P $(D_2D_1)^{N/2}$ immersed in free space, shown in Fig.1. There are *N* stacks where each *N/2* period or stack composed of dielectrics mediums indexed (D_1, D_2) and a magnetized cold plasma layer (MCP) layer indexed *P*. Each layer has a thickness d_l, and refractive index n_l. In order to find the formulation of the structure, we assumed that the incident electromagnetic wave from air to the dielectric and plasma layer, the layers are on the *x-y* plane and the *z* direction is normal to layer interface.

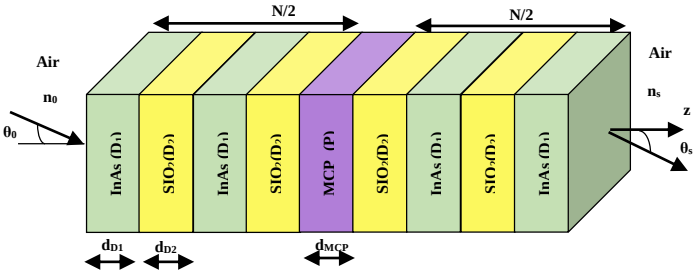

Fig. 1. Schematic representation of the 1D-PC Dielectric-Dielectric defected by MCP material

The refractive index profile of magnetized cold plasma *P* and Dielectric mediums (D_1, D_2) can be given as:

$$\begin{cases} n_{D1} = n_{InAs} = \sqrt{\varepsilon_{D1}} \\ n_{D2} = n_{SiO2} = \sqrt{\varepsilon_{D2}} \\ n_P = n_{MCP} = \sqrt{\varepsilon_P} \end{cases} \quad (1)$$

where ε_P, ε_{D1}, ε_{D2}, n_P, n_{D1}, n_{D2} denote respectively the relatives permittivity and refractive indices of *P*, D_1, D_2 mediums.

From the two fluid models, the complex permittivity of MCP layer *P* is a function of frequency ω and static magnetic field $\tilde{B}$ and can be expressed as [13]:

$$\varepsilon_P(\omega) = 1 - \frac{\omega_{pe}^2}{\omega^2\left(1 - i\frac{\gamma}{\omega} \pm \frac{\omega_{le}}{\omega}\right)} \quad (2)$$

where ω, γ, ω_{pe} and ω_{le} are the angular frequency, the effective collision frequency, plasma and gyro-frequency, respectively. ω_{pe} and ω_{le} are given by:

$$\omega_{pe} = \sqrt{n_e e^2 / m\varepsilon_0} \quad (3)$$

$$\omega_{le} = e\tilde{B}/m \quad (4)$$

where *e*, *m*, n_e and ε_0 are the electronic charge, the electronic mass, the electron density and the free-space permittivity, respectively.

In Eq. (2), the sign (±) in ω_{le} corresponds to the application of a positive or negative external magnetic field, in other words, the static magnetic field is applied in a *d*+*z* or *d*-*z* direction [13].

Based on Maxwell's equations and Boundary conditions, using the boundary conditions and the condition of continuity of *E* and *H* fields we can find out the relationship between the fields (1D-PC) structure consisting of *l* layer, this relation is already exposed by [14-15]:

$$\begin{bmatrix} E_1 \\ H_1 \end{bmatrix} = M_1 M_2 \dots\dots M_N \dots\dots M_{2N} \begin{bmatrix} E_l \\ H_l \end{bmatrix} \quad (5)$$

The matrix M_{l-1} of the l^{th} layer can be written in the form:

$$M_{(l-1)} = \begin{bmatrix} \cos(\delta_{(l-1)}) & i\,\gamma_{(l-1)}\sin(\delta_{(l-1)}) \\ i\,\gamma_{(l-1)}{}^{-1}\sin(\delta_{(l-1)}) & \cos(\delta_{(l-1)}) \end{bmatrix} \quad (6)$$

$\delta_{(l-1)}$ and $\gamma_{(l-1)}$ being the matrix parameters as a function of the incident angle of light, the optical constants and the thickness of the layer are expressed as:

$$\delta_{(l-1)} = k_{(l-1)}.d_{(l-1)}.\cos\theta_{(l-1)} \quad (7)$$

$$\gamma_{(l-1)} = \begin{cases} \frac{\eta_{(l-1)}}{\cos\theta_{(l-1)}} & \text{TE mode} \\ \eta_{(l-1)}\cos\theta_{(l-1)} & \text{TM mode} \end{cases} \quad (8)$$

where the wave numbers and intrinsic impedances are:

$$k_l = \omega\sqrt{\varepsilon_0\mu_0\varepsilon_l\mu_l} \quad (9)$$

$$\eta_l = \frac{k_l}{\omega\varepsilon_l\varepsilon_0} = \sqrt{\frac{\mu_0\mu_l}{\varepsilon_0\varepsilon_l}} \quad (10)$$

where ε_0, μ_0, ε_l and μ_l are the free space permittivity, free space permeability, relative permittivity, and relative permeability ($\mu_l = 1$),respectively.

Considering the transmission matrix of each layer, we can obtain the transmission matrix of the entire structure. For *l* number of multilayer's; the corresponding transfer matrix can be defined as a product of matrices, and is obtained from the symmetric PBG structure,

$$M = \prod_{k=1}^{(2N)} M_k = \begin{bmatrix} m_{11} & m_{12} \\ m_{21} & m_{22} \end{bmatrix} \quad (11)$$

The product of matrices of (1D-PC) structure with defect layer can be then written as follows [16]:

$$M = \prod_{k=1}^{(2N+1)} M_k = (M_{D1}M_{D2})^N M_P (M_{D2}M_{D1})^{(2N+1)} = \begin{bmatrix} m_{11} & m_{12} \\ m_{21} & m_{22} \end{bmatrix} \quad (12)$$

where M_{D1}, M_{D2} and M_P are the transfer matrixes of the Dielectric and the defect MCP layer. m_{11}, m_{12}, m_{21} and m_{22} are the complex numbers.

The transmittance *t* and reflectance *r* are defined as the ratios of the fluxes of the transmitted and reflected waves, respectively, to the flux of the incident wave. After a few derivations, the total reflection and transmission coefficients are given by [17]:

$$r = \frac{(m_{11} + p_s^{-1}m_{12})p_0^{-1} - (m_{21} + p_s^{-1}m_{22})}{(m_{11} + p_s^{-1}m_{12})p_0^{-1} + (m_{21} + p_s^{-1}m_{22})} \quad (13)$$

$$t = \frac{2.p_0^{-1}}{(m_{11} + p_s^{-1}m_{12})p_i^{-1} + (m_{21} + p_s^{-1}m_{22})} \quad (14)$$

Here p_0 and p_s are the first and last medium of the structure which are given by:

$$p_s^{-1} = \begin{cases} \frac{\eta_s \cos\theta_s}{Z_0} & \text{TE mode} \\ \frac{\eta_s}{Z_0 \cos\theta_s} & \text{TM mode} \end{cases} \quad (15)$$

$$p_0^{-1} = \begin{cases} \frac{\eta_0 \cos\theta_0}{Z_0} & \text{TE mode} \\ \frac{\eta_0}{Z_0 \cos\theta_i} & \text{TM mode} \end{cases} \quad (16)$$

where $Z_0 = \sqrt{\mu_0/\varepsilon_0}$

III. NUMERICAL RESULTS

A. The transmittance of the defective asymmetric & symmetrical structure

To analyze the structure based on InAs/SiO_2 in symmetric and asymmetric by the TMM method, we plotted the transmittance spectrum in Fig.2, using the parameters shown in TABLE I.

TABLE I. THE PARAMETERS OF THE MATERIALS USED [13, 18].

Layer	ε	μ	d [mm]	B [T]	n_e [m^{-3}]	γ [Hz]
InAs	3.3842	1.0	3.1	-	-	-
SiO_2	1.4672	1.0	7.4	-	-	-
MCP	-	1.0	-	0.4	10^{18}	10^7

The transmittance of the asymmetric structure $(InAs/SiO_2)^2$ MCP $(InAs/SiO_2)^2$, shows a large difference as shown in Fig.2a. Likewise, the transmittance of the symmetrical structure $(InAs/SiO_2)^2$ MCP $(SiO_2/InAs)^2$ is analyzed which shows, that the band gap is divided into two bands due to the symmetrical arrangement Fig.2b.

The bandwidth of the defective symmetrical structure increases relative to the asymmetric structure due to the existing defect mode. The transmission fault peak of the symmetrical structure is used in many applications such as filters and laser resonators.

Next, we focus on the study of the symmetrical structure with an MCP plasma defect layer and with the variation of the angle of incidence and parameters of the plasma. As we know that the optical property of the material changes by changing the refractive index of the material as well as the angle of incidence.

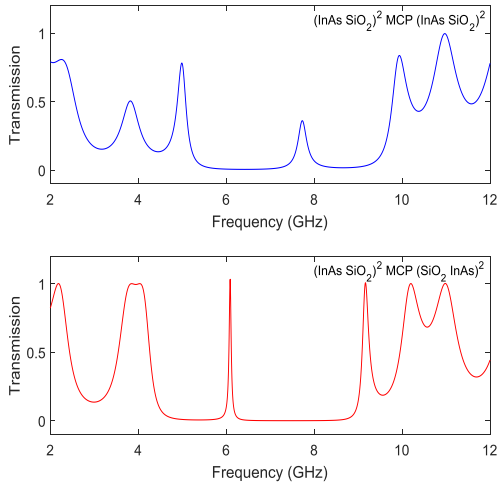

Fig. 2. Transmission spectra as a function of frequency; a) Asymmetric periodic structure, b) Symmetric periodic structure.

B. Effect of varying the angle of incidence

The variation of the angle of incidence plays a large role in the variations of the optical properties of the defective periodic structure considered. Therefore, the transmittance of 1D-PC symmetrical of $InAs/SiO_2$ with a MCP defect is analyzed as a function of the variation of the angle of incidence $\theta=0$, $\theta=\pi/6$, $\theta=\pi/4$ and $\theta=\pi/3$ Fig.3.

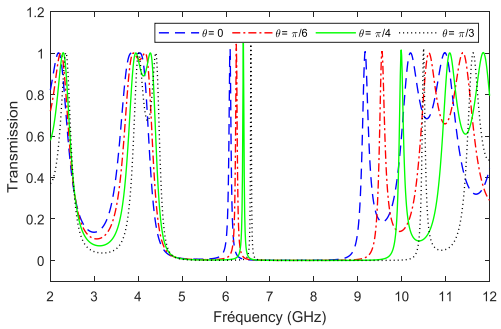

Fig. 3. Transmission spectra of the symmetric 1D-PC structure as a function of frequency for different values of incidence angle.

Fig3 and TABLE II show that the faulty transmission peaks and the forbidden bands are shifted to the higher frequency to increase the value of the angles of incidence and thus form a multiband filter, due to the composite behavior of the dielectric material and plasma. The transmittance shows that the large transmittance shift is obtained for a large value of the angle of incidence $\theta = \pi / 3$.

TABLE II. THE RESONANCE PEAKS AND THE WIDTHS OF THE PBG S OF THE TRANSMISSION OF THE SYMMETRICAL 1D-PC STRUCTURE, FOR THE TE MODE.

θ	**0**	**π/6**	**π/4**	**π/3**
fr [Ghz]	6.096	6.231	6.396	6.562
PBG [Ghz]	5.165	5.361	5.691	6.084

These results can be compared to a 1D-PC structure composed of Dielectric-superconductor with and without the defect layer [19], and analyzed the defect peak which is shifted to a higher frequency when the angle θ. The incidence is increasing, but the multichannel behavior has not materialized. Therefore, we have proposed very simple $InAs/SiO_2$ adhesive materials with an MCP defect layer and a period N=4, model easy to achieve [11, 12].

Our transmittance calculations of a one-dimensional symmetrical structure of Indium Arsenide (InAs), Silicon Dioxide (SiO_2) with an MCP plasma defect layer were better, for multi-channel filter applications having tenability property.

C. Effect of variation of plasma electron density

Electron density can change the frequency of plasma (MCP) and plays a big role in changing its refractive index. In Fig4, we analyze the frequency-dependent transmittance of the periodic multilayer structure of indium arsenide and silicon dioxide with a MCP defect layer, for different values of the electron density.

The transmittance is shifted to low frequencies as the electron density increases due to the decrease in the refractive index value of the plasma. Likewise, the transmission peak is slightly high and shifted towards low frequencies as the electron density increases and the optical constant of the plasma material changes TABLE III. Therefore, the electrical permittivity of the MCP plasma material changes due to the electron density. The results obtained from the transmittance appear as a tunable multichannel filter in the microwave region.

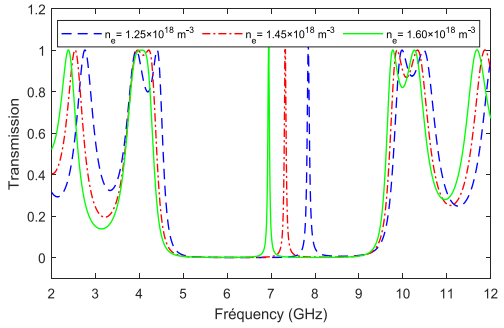

Fig. 4. Transmission spectra as a function of the frequency of the symmetric 1D-PC periodic structure for different values of the electron density of the plasma.

TABLE III. THE RESONANCE PEAKS AND THE TRANSMISSION PBGS FOR DIFFERENT VALUES OF THE ELECTRON DENSITY OF THE PLASMA.

n_e [m^{-3}]	1.25×10^{18}	1.45×10^{18}	1.60×10^{18}
fr [Ghz]	7.853	7.327	6.937
PBG [Ghz]	5.591	5.646	5.586

D. Effect of magnetic field

The electrical permittivity of MCP plasma can change by the external magnetic field because the gyroscopic frequency depends on the magnetic field. The external magnetic field changes the refractive index of the MCP plasma.

This means that the transmittance of the periodic structure containing plasma also varies with the magnetic field in MCP plasma. We have studied the transmittance of the periodic structure of InAs/SiO_2 with a defective layer of MCP plasma as a function of the variation of the applied external magnetic field, B = 0.1T, B = 0.2T, B = 0.3T, this is shown in Fig. 5. The transmittance as a function of the frequency and the variation of the external magnetic field was analyzed. The transmission peak has shifted to the higher frequency due to the effect of the MCP material at optical constant TABLE IV. As the magnetic field increases, each band is shifted to the highest frequency corresponding to the value of the magnetic field. This shows that the tunable multichannel filter is obtained by an external magnetic field for microwave devices.

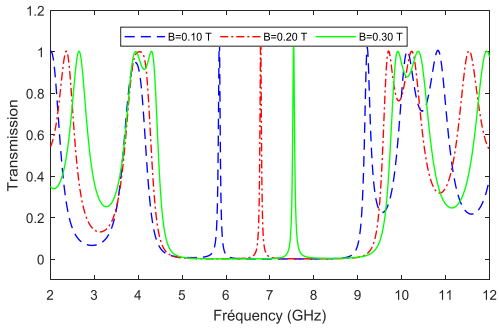

Fig. 5. Transmission spectra as a function of frequency of the symmetric 1D-PC periodic structure for different values of the magnetic field.

These results also compare a new tunable filter comprising a fault mode of the TE wave of a one-dimensional photonic crystal doped with a magnetized plasma and the transmission spectra of the periodic structure of dielectric (SiO_2) and dielectric (air) materials. The transmittance spectra as a function of the frequency are analyzed with MCP plasma defect on the variation of the magnetic field, the density of the plasma and the electron density, their interest is in the tunable filter [20].

TABLE IV. THE RESONANCE PEAKS AND PBG S OF THE TRANSMISSION FOR DIFFERENT VALUES OF THE MAGNETIC FIELD.

B	1.0	2.0	3.0
fr [Ghz]	5.841	6.787	7.538
PBG [Ghz]	5.21	5.586	5.661

E. Resonant structures and the quality factor Q

In Fig6, we have reported the variation of the transmission spectra as a function of the frequency of a symmetrically shaped 1D-PC structure, the aim of which is to study the relationship between the number of fault layers and the fault modes.

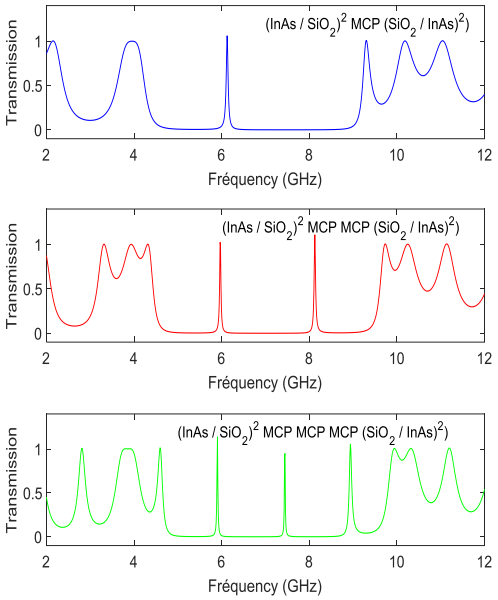

Fig. 6. Transmission spectra as a function of the frequency of the symmetric 1D-PC periodic structure for deferent numbers of defect layers, (θ = 0, TE mode, $\gamma = 1.0 \times 10^7$, $n_e = 1.0 \times 10^{18}$, B = 0.30 T); (dInAs = 3.1mm, $dSiO_2$ = 7.4mm, dMCP = 12.0mm); (nInAs = 3.3842, $nSiO_2$ = 1.4672).

TABLE V. RESONANT FREQUENCY AND QUALITY FACTOR Q FOR DIFFERENT CONFIGURATIONS.

Configuration	**Peaks**	**f_r**	**Q**
$(InAs\text{-}SiO_2)^2$ MCP $(SiO_2\text{- }InAs)^2$	1st Peak	6.126	1531.5
$(InAs\text{-}SiO_2)^2$ MCP MCP $(SiO_2\text{- }InAs)^2$	1st Peak	5.976	181.1
	2nd Peak	8.123	203.1
$(InAs\text{-}SiO_2)^2$ MCP MCP MCP $(SiO_2\text{-}InAs)^2$	1st Peak	5.901	85.5
	2nd Peak	7.447	354.6
	3rd Peak	8.934	124.1

Our results imply that the number of defects can be increased by adding defective layers in the 1D-PC structure of the symmetric shape, and for the filter to be more selective, we choose the first configuration or Q = 1531.5 Table V.

IV. CONCLUSION

In this work, a new design and analysis of one-dimensional defective photonic crystal structure, containing the magnetized cold plasma and Dielectric layer are presented. Theoretical results in terms of the transmission spectra for the various (1D-PCs) configurations were presented, and theoretically investigated by the transfer matrix method (TMM). Current simulations show that the width of the photonic band gap can be adjusted by modifying the magnetic field. In case of fixed the MCP layer's thickness, also magnetic field could increase the width of the phonic band gap. The number of the defect modes can be controlled by adjusting the number of defect layers in the structure. Therefore, the proposed structure configurations may be of potential use and interest in many applications such as optical communication selective filters.

RÉFÉRENCES

[1] B. Guo, "Photonic band gap structures of obliquely incident electromagnetic wave propagation in a one-dimension absorptive plasma photonic crystal," vol. 16, no. 4, p. 043508, 2009.

[2] H. Hojo and A. Mase, «Electromagnetic-wave transmittance characteristics in one-dimensional plasma photonic crystals," vol. 8, p. 477-479, 2009.

[3] W. Fan and L. Dong, «Tunable one-dimensional plasma photonic crystals in dielectric barrier discharge," vol. 17, no. 7, p. 073506, 2010.

[4] L. Qi, "The absorbing properties of one-dimensional plasma photonic crystals," vol. 82, no. 1, 2016.

[5] M. M. Abadla et al., "Properties of ternary photonic crystal consisting of dielectric/plasma/dielectric as a lattice period," vol. 185, p. 784-793, 2019.

[6] L. Qi, Z. Yang and T. Fu, "Defect modes in one-dimensional magnetized plasma photonic crystals with a dielectric defect layer," vol. 19, no. 1, p. 012509, 2012.

[7] Aly, A. H., Elsayed, H. A., Ameen, A. A., & Mohamed, S. H. "Tunable properties of one-dimensional photonic crystals that incorporate a defect layer of a magnetized plasma," vol. 31, no. 31, p. 1750239, 2017.

[8] T.-W. Chang, J.-R. C. Chien and C.-J. Wu, "Magnetic-field tunable multichannel filter in a plasma photonic crystal at microwave frequencies," vol. 55, no. 4, p. 943-946, 2016.

[9] A. Aghajamali, "Transmittance properties in a magnetized cold plasma–superconductor periodic multilayer," vol. 55, no. 23, p. 6336-6340, 2016.

[10] Chettah, C., Barkat, O. & Chaabi, A. Tunable Properties of Optical Selective Filters Based on One-Dimensional Plasma Superconductor Photonic Crystal. J Supercond Nov Magn (2021). https://doi.org/10.1007/s10948-021-05891-1

[11] Parm, I. O., Roh, Y., Hong, B., Park, C. S., & Yi, J., "The improvement of the SiO_2/InAs interface properties with the aid of fast electron irradiation in a direct current sputter deposition system," vol. 172, no. 3-4, p. 295-300, 2001.

[12] N. Valisheva et al., "Electrical properties of InAs-SiO_2-In 2 O 3 MIS structures with a modified interface," vol. 38, no. 2, p. 87-94, 2009.

[13] H. G. Booker, Cold Plasma Waves (Springer-Verlag, 1984), pp. 23–25.

[14] Scotognella, F.:Four-material one dimensional photonic crystals. Elsevier, Optical Materials. 34, 1610-1613 (2012)

[15] Oraizi H., Abdolali, A.:Several theorems for reflection and transmission coefficients of plane wave incidence on planar multilayer metamaterial structures. IET Microw. Antennas Propag. 4, 1870–1879(2010)

[16] Aly, A. H., Sabra, W., Abdel-Rahman, E.: Investigation of the transmittance in superconducting photonic crystal. Progress in Electromagnetics Research Symposium Proceedings, KL, MALAYSIA, March 27-30 (2012)

[17] Wu, C.-J. : Transmission and Reflection in a Periodic Superconductor/Dielectric Film Multilayer Structure. Journal of Electromagnetic Waves and Applications. 19, 1991–1996 (2005)

[18] D. E. Aspnes and A. Studna, "Dielectric functions and optical parameters of si, ge, gap, gaas, gasb, inp, inas, and insb from 1.5 to 6.0 ev," vol. 27, no. 2, p. 985, 1983.

[19] B. Mamri and O. Barkat, "Design of a Selective Filter Based on One-dimensional Superconductor Photonic Crystal," vol. 32, no. 11, p. 3397-3405, 2019.

[20] Kong, X., Liu, S., Zhang, H., & Li, C., "A novel tunable filter featuring defect mode of the TE wave from one-dimensional photonic crystals doped by magnetized plasma," vol. 17, no. 10, p. 103506, 2010.